

Subtle Morphology Control with Binary Additives for High-Efficiency Non-Fullerene Acceptor Organic Solar Cells

Yunqian Ding,^{||} Xin Zhang,^{||} Huanran Feng, Xin Ke, Lingxian Meng, Yanna Sun, Ziqi Guo, Yao Cai, Cancan Jiao, Xiangjian Wan, Chenxi Li, Nan Zheng, Zengqi Xie, and Yongsheng Chen*



Cite This: *ACS Appl. Mater. Interfaces* 2020, 12, 27425–27432



Read Online

ACCESS |



Metrics & More



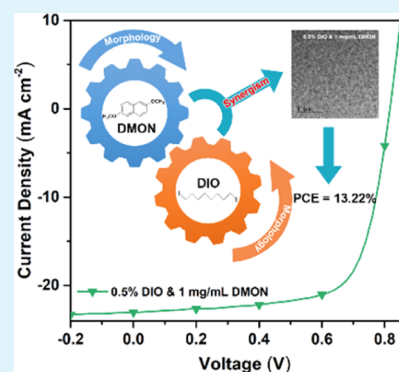
Article Recommendations



Supporting Information

ABSTRACT: Adding an additive is one of the effective strategies to fine-tune active layer morphology and improve performance of organic solar cells. In this work, a binary additive 1,8-diiodooctane (DIO) and 2,6-dimethoxynaphthalene (DMON) to optimize the morphology of PBDB-T:TTC8-O1-4F-based devices is reported. With the binary additive, a power conversion efficiency (PCE) of 13.22% was achieved, which is higher than those of devices using DIO (12.05%) or DMON (11.19%) individually. Comparison studies demonstrate that DIO can induce the acceptor TTC8-O1-4F to form ordered packing, while DMON can inhibit excessive aggregation of the donor and acceptor. With the synergistic effect of these two additives, the PBDB-T:TTC8-O1-4F blend film with DIO and DMON exhibits a suitable phase separation and crystallite size, leading to a high short-circuit current density (J_{sc}) of 23.04 mA·cm⁻² and a fill factor of 0.703 and thus improved PCE.

KEYWORDS: organic solar cells, non-fullerene acceptor, binary additives, synergistic effect



INTRODUCTION

In the past decade, organic solar cells (OSCs) have made great progress, especially after the rapid development of non-fullerene acceptors (NFAs). Presently, power conversion efficiencies (PCEs) with breakthrough values of 16–18% have been achieved, thanks to the new active layer material design and device optimization.^{1–11} In contrast to the much enthusiasm on the innovation of new active layer materials, for example, NFAs with the A–D–A architecture,^{12–27} less attention has been paid to the morphology control, which has been proved to be of great importance to obtain high-performance devices.^{28–37} The ideal morphology of active layers should have nanoscale phase separation with a good bicontinuous interpenetrating network.³⁸ To date, many efficient methods for morphology control have been developed, such as host solvent selection,^{34,39,40} thermal or solvent vapor annealing,^{26,30} additives,^{31,32,41–43} and so forth. Among them, additives have been widely used and demonstrated great success in the morphology control. For example, solvent additives, such as 1,8-diiodooctane (DIO),^{42,43} *N*-methyl pyrrolidone (NMP),^{44,45} and 1-chloronaphthalene (CN),^{41,46} have been widely used to optimize the bulk morphologies of active layers to produce suitable phase separation. Most of the additives are liquid with different solubilities for donors and acceptors and have higher boiling points than the host solvent of active layers, which can generally render nanoscale phase separation and improve crystallization for active layers.^{28,38} Besides liquid additives,

solid molecules can also be used as additives to optimize morphology, which have been realized in recent work of Hou et al.^{47,48} It has been found that the volatilizable solid additives can enhance the intermolecular π – π stacking and the charge transport of IT-4F. Note that a single additive is used in most cases for morphology optimization. In contrast, only a few cases of binary additives have been reported, although promising results would be expected owing to the synergistic effect or subtle balanced influence of the two additives.^{44,49–54} For example, Wang et al. reported the FTAZ:IDCIC-based device using the 0.25% CN and DIO ($V_{CN}/V_{DIO} = 1:1$) as additives.⁵² A PCE of 13.58% was achieved, which was higher than those of single additive devices (9.76 or 11.81%) because of the balanced impact of DIO and CN. Zhang et al. employed binary additives of 1.5% DIO and 1.5% NMP to tune morphology of the PTB7-Th:PC₇₁BM blend film and a PCE of 10.8% was obtained with the binary additives, owing to the improved domain purity and less bimolecular recombination in the optimized device.⁴⁴

Herein, we reported the results of a binary additive composed of a liquid additive DIO and a solid additive 2,6-

Received: March 22, 2020

Accepted: May 29, 2020

Published: May 29, 2020



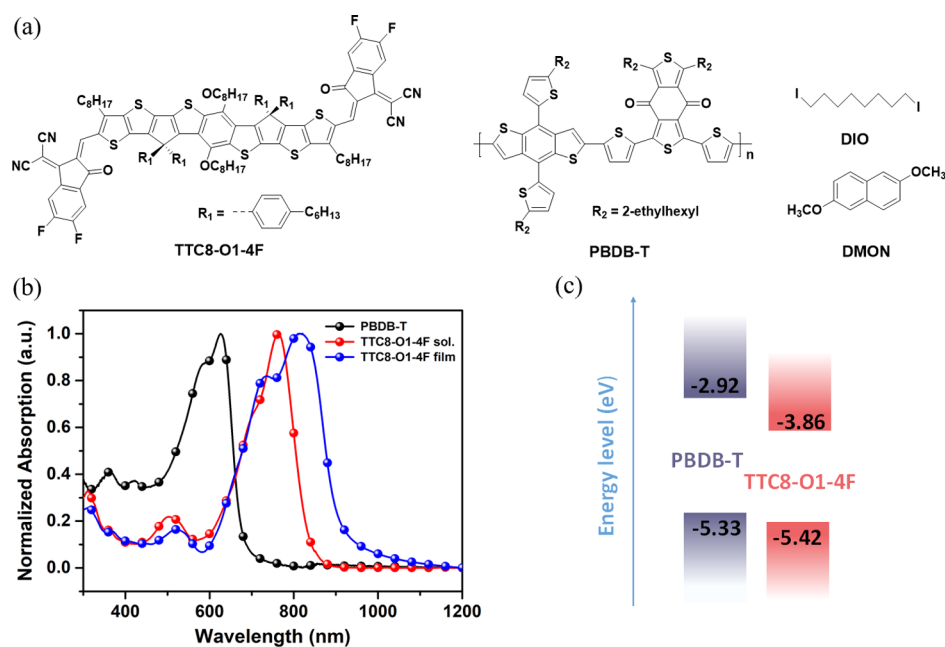


Figure 1. (a) Chemical structures of TTC8-O1-4F, PBDB-T, DIO, and DMON; (b) normalized optical absorption spectra of PBDB-T and TTC8-O1-4F; and (c) HOMO/LUMO energy levels of PBDB-T and TTC8-O1-4F.

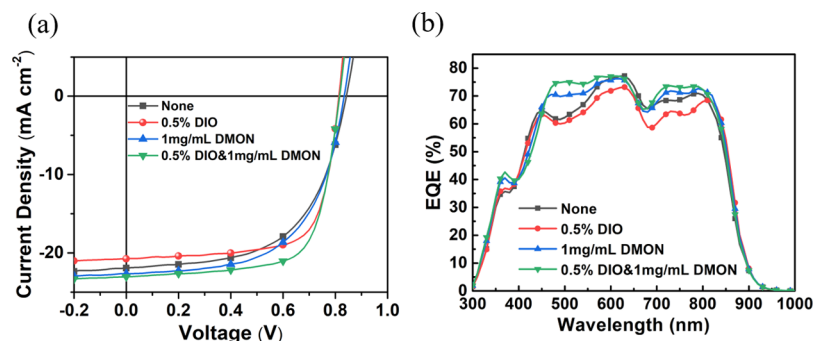


Figure 2. (a) J - V curves and (b) EQE curves of the best PCE-based PBDB-T:TTC8-O1-4F under different conditions.

dimethoxynaphthalene (DMON) for an OSC based on PBDB-T and a new acceptor TTC8-O1-4F. TTC8-O1-4F has been designed based on the acceptor OBTT-4F we reported previously by introducing octyl chains on the backbone, as shown in Figure 1a.^{55,56} With device optimization using this binary additive, PBDB-T:TTC8-O1-4F-based devices gave a PCE of 13.22%, which is higher than that of devices using additive DIO (12.05%) or DMON (11.19%) individually. Comparison studies indicate that the addition of DIO can induce the acceptor TTC8-O1-4F to form ordered packing, while the addition of DMON can inhibit excessive aggregation of the donor and acceptor. With the synergistic effect of these two additives, the blend film of PBDB-T:TTC8-O1-4F could have a more suitable morphology, leading to a less bimolecular recombination, relatively higher PCE. The results indicate that the binary additive approach with a liquid and a solid component can be used as one of the potential strategies for morphology optimization.

RESULTS AND DISCUSSION

Optical Properties and Energy Levels of TTC8-O1-4F.

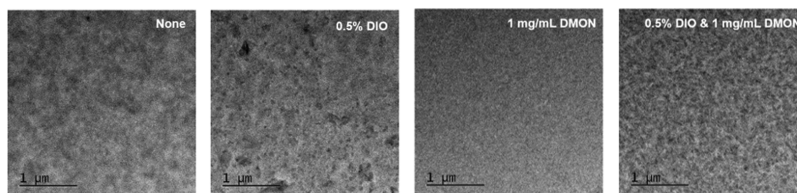
The chemical structures of active layer materials and the two additives of DIO and DMON used in this study are shown in

Figure 1a. The detailed synthesis and characterization of TTC8-O1-4F are provided in the Supporting Information. Thermogravimetric analysis (TGA) suggests that TTC8-O1-4F has excellent thermal stability up to 326 °C under a N₂ atmosphere (Figure S3a). The differential scanning calorimetry (DSC) characteristics of TTC8-O1-4F have also been tested. As depicted in Figure S3b, TTC8-O1-4F exhibits a sharp exothermic peak at 158 °C, which is assigned to the behavior of molecular crystallization. The absorption spectra of TTC8-O1-4F are shown in Figure 1b. In the dilute chlorobenzene solution, TTC8-O1-4F exhibits a broad absorption of 600–900 nm with a maximum peak at 763 nm. In the solid film, TTC8-O1-4F displays a red-shifted absorption by 55 nm with the absorption edge around 945 nm. The highest occupied molecular orbital (HOMO) and lowest unoccupied molecular orbital (LUMO) levels of TTC8-O1-4F were measured by cyclic voltammetry (CV) to be −5.42 and −3.86 eV (Figure S2), respectively. For the new solid additive DMON, its film shows absorption in the range 300–500 nm with a peak around 350 nm (Figure S4a). Note that DMON is a volatilizable solid, which could be confirmed from the disappearance of absorption of DMON on the quartz substrate after thermal annealing under 140 °C (Figure S4b).

Table 1. Photovoltaic Parameters of the Optimized Devices Based on PBDB-T:TTC8-O1-4F Under Different Conditions

additive ^a	V_{oc} ^b [V]	FF ^{cb}	J_{sc} ^b [$\text{mA}\cdot\text{cm}^{-2}$]	PCE ^{bc} [%]	J_{EQE} ^c [$\text{mA}\cdot\text{cm}^{-2}$]
none	0.842(0.844 ± 0.005)	0.582(0.589 ± 0.016)	21.93(21.55 ± 0.50)	10.75(10.70 ± 0.11)	20.96
0.5% DIO	0.814(0.813 ± 0.003)	0.714(0.708 ± 0.015)	20.73(20.57 ± 0.35)	12.05(11.86 ± 0.24)	20.22
1 mg/mL DMON	0.834(0.836 ± 0.005)	0.593(0.581 ± 0.019)	22.63(22.66 ± 0.50)	11.19(11.02 ± 0.17)	21.61
0.5% DIO & 1 mg/mL DMON	0.816(0.815 ± 0.004)	0.703(0.692 ± 0.010)	23.04(22.84 ± 0.35)	13.22(12.74 ± 0.43)	21.92

^a140 °C for 10 min after film coating. ^bThe average values in parentheses were obtained from 10 devices. ^cThe J_{sc} values integrated from EQE spectra.

**Figure 3.** TEM images for different conditions of the blend films based on PBDB-T:TTC8-O1-4F.

Photovoltaic Properties. OSC devices were fabricated using an inverted device structure of indium tin oxide (ITO)/ZnO/PBDB-T/TTC8-O1-4F/MoO_x/Ag. With complementary absorption and matched energy levels, PBDB-T was selected as the donor material (Figure 1b,c and Table S1).⁵⁷ Detailed device fabrication and optimization conditions are given in the Supporting Information. The current density–voltage (J – V) curves of the optimal devices are shown in Figure 2a, and the corresponding photovoltaic parameters are listed in Table 1. We first fabricated the PBDB-T:TTC8-O1-4F-based device without any additive, which gave an optimized PCE of 10.75% with an open-circuit voltage (V_{oc}) of 0.842 V, a J_{sc} of 21.93 $\text{mA}\cdot\text{cm}^{-2}$, and a low fill factor (FF) of 0.582. Then, different amounts of DIO, DMON, and DIO and DMON were added into the solution of PBDB-T:TTC8-O1-4F to fabricate OSC devices and the detailed photovoltaic parameters are provided in Tables S3–S7. Compared with the control device without any additive, when 0.5 vol % DIO was added, the device showed an improved PCE of 12.05% with an improved FF of 0.714 but slightly decreased V_{oc} and J_{sc} values. In contrast, when 1 mg/mL DMON was added, the device exhibited a slightly enhanced PCE of 11.19% with an increase in J_{sc} nearly unchanged V_{oc} and FF. When the binary additive (0.5% DIO and 1 mg/mL DMON) was used, the device demonstrated a higher PCE of 13.22% with a V_{oc} of 0.816 V, a J_{sc} of 23.04 $\text{mA}\cdot\text{cm}^{-2}$, and an FF of 0.703. As shown in Figure 2b, higher external quantum efficiency (EQE) values in the wide range of 450–830 nm were obtained for the device with binary additives compared with the control and DIO- and DMON-only devices, in which the integrated current was consistent with the values from J – V curves (Table 1). Surprisingly, as shown in Table 1, the improved performance of the device with binary additives is attributed to the increased FF and J_{sc} compared with the control device without an additive.

Morphology Studies. Compared with the results from the devices with an individual additive, the impressive enhancement due to binary additives should come from either a combined or synergistic effect of the two additives on morphology change/optimization of the active layer. Thus, a series of studies of the corresponding morphology were carried out. The morphology of the PBDB-T:TTC8-O1-4F blend films with individual and binary additives was first compared by transmission electron microscopy (TEM) (Figure 3).⁵⁸ As shown in Figure 3, there exists fiber-like aggregation in the

control blend film without any additive. With only the additive DIO, the fiber-like domains are increased with clear aggregation compared with the control blend film. This morphology is favorable for the charge transport and thus leads to a high FF over 0.710. However, it could decrease the interfaces of donor and acceptor and suppress charge separation^{28,32,33} and thus slightly decrease the J_{sc} value (Table 1). With DMON only as an additive, a uniform and smooth surface morphology is formed with nearly no fiber-like domains as in the control and DIO-only films. In this case, the increased interface between the donor and acceptor with decreased domain size could render effective charge dissociation and contribute to the enhancement of J_{sc} , but the charge transport would be impacted, leading to low FF.^{31,33} With the binary additive of DIO and DMON, the blend film shows a uniformly distributed nanostructure with fiber-like interpenetrating network, which is favorable for exciton dissociation and charge transport and thus enabling its high J_{sc} and FF.

Grazing incidence wide-angle X-ray scattering (GIWAXS) was used to study the molecular orientation and packing behavior in the blend films of PBDB-T:TTC8-O1-4F with and without additives.^{33,59} The quantitative results for the morphology and some important results are summarized in Table 2. As shown in Figure 4a,b, for the control blend film without any additive, the peaks located at 0.29 \AA^{-1} in the in-plane (IP) direction and 1.73 \AA^{-1} in the out-of-plane (OOP) direction are assigned to the (100) lamellar and (010) π – π

Table 2. Summary of the GIWAXS Parameters for the Blend Films

additive	q_z (100) [\AA^{-1}] ^a	d_{100} [\AA]	q_z (010) [\AA^{-1}] ^b	d_{010} [\AA]	fwhm [\AA^{-1}] ^c	CCL [\AA] ^d
none	0.29	21.67	1.73	3.63	0.237	26.5
0.5% DIO	0.33	19.04	1.77	3.55	0.195	32.3
1 mg/mL DMON	0.29	21.67	1.72	3.65	0.368	17.1
0.5% DIO & 1 mg/mL DMON	0.32	19.63	1.74	3.61	0.214	29.3

^aThe (100) diffraction peak in the IP direction. ^bThe (010) diffraction peak in the OOP direction. ^cFull width at half-maximum by Gaussian fitting. ^dCCL estimated from Scherrer's equation (CCL = $2\pi k$ fwhm⁻¹).

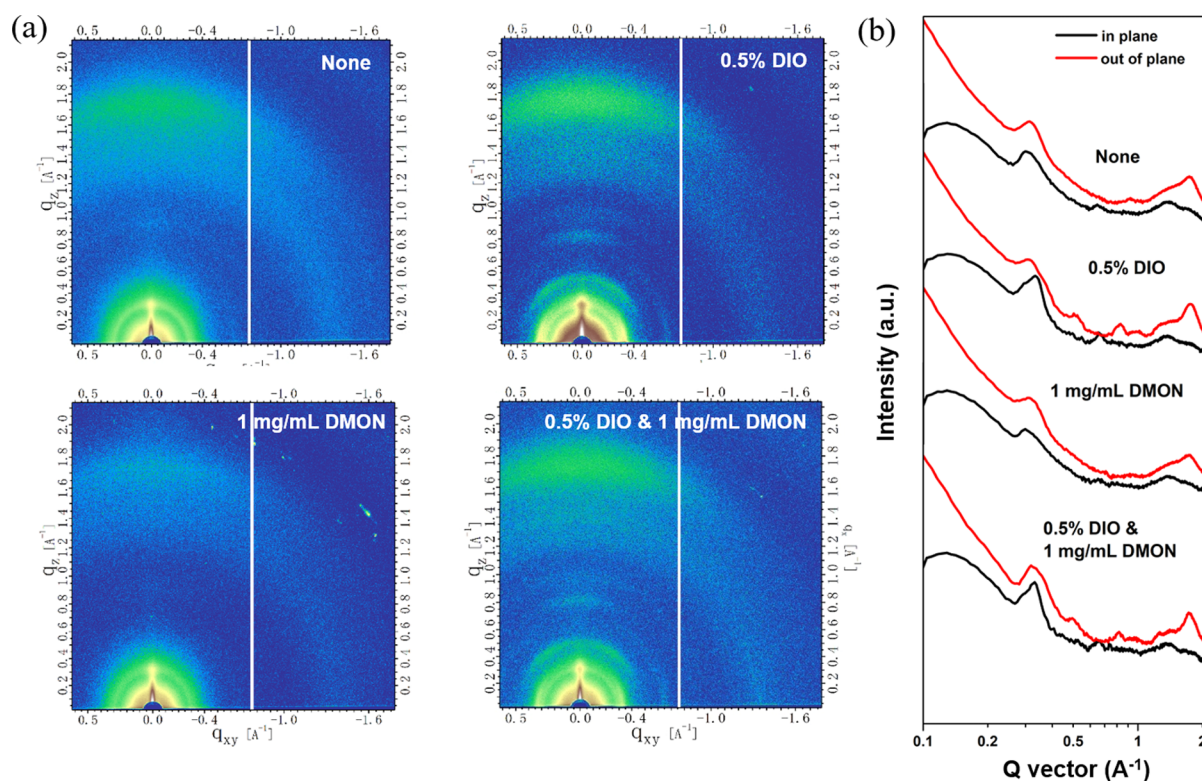


Figure 4. (a) 2D GIWAXS patterns for PBDB-T:TTC8-O1-4F blend films without or with additives. (b) Corresponding GIWAXS intensity profiles along the IP and OOP directions.

stacking scattering, corresponding to the lamellar and π - π stacking d -spacing of 21.67 and 3.63 \AA of the donor PBDB-T, respectively. This is consistent with the neat PBDB-T film (Figure S6). These results indicate that TTC8-O1-4F does not tend to form ordered packing in the control blending film. With only 0.5% DIO as the additive, the blend film exhibits much stronger crystallinity with clear lamellar and π - π stacking peaks at 0.33 and 1.77 \AA^{-1} , corresponding to the lamellar and π - π stacking d -spacing of 19.04 and 3.55 \AA , respectively. Clearly, the addition of DIO is contributed to the ordered packing of PBDB-T and TTC8-O1-4F, especially TTC8-O1-4F, because significant red-shifted absorption of TTC8-O1-4F could be observed in the blend film absorption (Figure S5). In contrast, the crystallinity of the blend film is significantly decreased when 1 mg/mL DMON was added, indicated by the decreased crystal coherence length (CCL) of 17.1 \AA and increased π - π stacking d -spacing of 3.65 \AA compared with the control film. With the binary additive of DIO and DMON, the π - π stacking d -spacing and CCL are calculated to be 3.61 and 29.3 \AA , respectively, which are between the values of the DIO-only and DMON-only blend film. This result is consistent with the absorption spectra of PBDB-T:TTC8-O1-4F-based blend films (Figure S5) and TEM results (Figure 3) under different additives. These results indicate that the binary additive with DIO and DMON help to form a subtly appropriate morphology with the suitable crystallite size, which is favorable for the high J_{sc} and FF in the OSC devices.

Based on the above mentioned detailed morphological characterization, the working mechanism for these binary additives is proposed. As shown in Figure 5, in the control blend film without any additive, TTC8-O1-4F is dispersed without much ordered packing, which might be caused by its

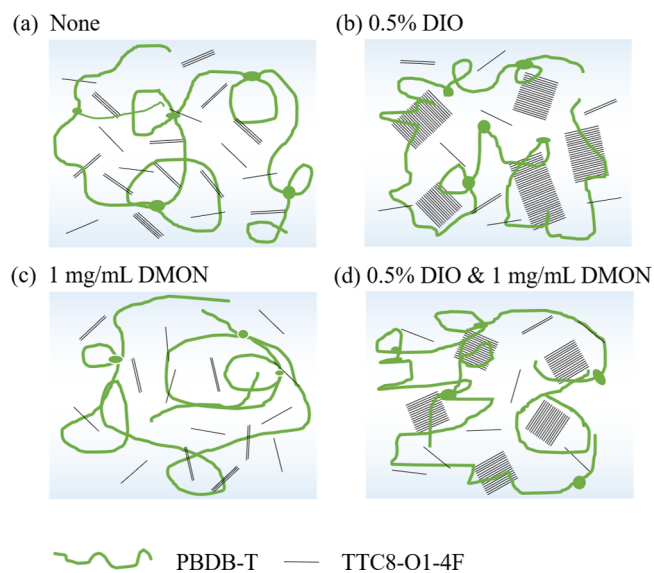


Figure 5. Schematic illustration of the working mechanism for PBDB-T:TTC8-O1-4F blend films (a) without an additive or with (b) DIO, (c) DMON, and (d) DIO and DMON.

good miscibility with the polymer. With only DIO as the additive, TTC8-O1-4F tends to form ordered packing with large phase separation, which is consistent with the results reported.^{25,29–32} In contrast, the solid DMON can be dispersed homogeneously in the donor and acceptor. After thermal annealing, it sublimates from the blend film and decreases the initially effective interaction of the donor and acceptor. With the binary additive of DIO and DMON, an equilibrium could be reached for the two reversed effect of the

two additives for the blend film and thus a preferred morphology with suitable phase separation and crystallite size can be obtained.

Charge Recombination and Transport Properties. The photocurrent density (J_{ph}) versus effective voltage (V_{eff}) curves were measured in order to study the charge generation and recombination behavior in the PBDB-T:TTC8-O1-4F-based device with/without an additive. The charge dissociation probability could be estimated with the value of J_{ph}/J_{sat} . Under short-circuit conditions, the closer the J_{ph}/J_{sat} is to 100%, the more efficient the charge dissociation becomes.^{60,61} As shown in Figure S7, the J_{ph}/J_{sat} ratio for the control, DIO, DMON, and DIO and DMON devices is 93, 91, 94, and 96%, respectively. The results indicate that the devices with 1 mg/mL DMON only and binary additives have high efficient charge dissociation, corresponding to their high J_{sc} 's. For studying the charge recombination properties in the devices, the incident light-intensity (P_{light}) dependence of J_{sc} was measured. The data were fitted to the power law: $J_{sc} \propto P_{light}^\alpha$. When α is closer to 1, less bimolecular recombination is implied (Figure S8).⁶² The α values are 0.960, 0.977, 0.964, and 0.972 for the control, DIO, DMON, and DIO and DMON devices, respectively. These results show less bimolecular recombination in the above mentioned devices, especially for the devices with DIO only and the binary additives, which is consistent with the high J_{sc} and FF for the corresponding devices. The transient photovoltage and photocurrent experiments were conducted to study the charge carrier lifetime and charge extraction life in the devices under different conditions. As shown in Figure S9, the results suggest that the device with the binary additives exhibits a slightly longer carrier lifetime (21.7 μ s) and a relatively shorter charge sweep out time (0.18 μ s) than that of devices using the additive DIO or DMON individually, which is correlated to a weaker recombination and the observed higher J_{sc} and FF in the DIO and DMON devices. Photoluminescence (PL) quenching experiments were also carried out to confirm the charge transfer behavior in the blend films. As shown in Figure S10, when excited at 585 nm, the PL intensities of the pure donor PBDB-T are significantly quenched in each blend film. When excited at 820 nm, the PL spectrum was more effectively quenched (nearly 96%) in the DIO and DMON film, suggesting more efficient charge transfer among the D–A interfaces for PBDB-T:TTC8-O1-4F blend films. To further investigate charge transport properties of each additives, the space charge-limited current method was used to measure the hole mobilities and electron mobilities (Figure S11).^{63,64} As shown in Table S2, the hole/electron mobilities are $1.90 \times 10^{-4}/9.25 \times 10^{-5}$, $1.62 \times 10^{-4}/1.54 \times 10^{-4}$, $2.49 \times 10^{-4}/1.32 \times 10^{-4}$, and $2.78 \times 10^{-4}/2.47 \times 10^{-4}$ $\text{cm}^2 \cdot \text{V}^{-1} \cdot \text{s}^{-1}$ for the control, DIO, DMON, and DIO and DMON devices, respectively. Among them, the devices with additives, particularly for the case of the binary additive, show overall improved and more balanced hole/electron mobilities, which benefits for the charge transport and produces high J_{sc} and FF in the device.

CONCLUSIONS

In summary, we have reported a binary additive (DIO and DMON) to improve the performance of PBDB-T:TTC8-O1-4F-based OSCs owing to the optimized active layer morphology. DIO and DMON each has different influence on the morphology of the PBDB-T:TTC8-O1-4F blend film. DIO induces ordered packing of the acceptor of TTC8-O1-4F,

while DMON suppresses the formation of over packing of the donor and acceptor. The binary additive of DIO and DMON produces a balanced and preferred morphology with suitable phase separation and crystallite size. With the binary additive, PBDB-T:TTC8-O1-4F-based OSCs afford an impressive PCE of 13.22%, which is higher than that of DIO-only (12.05%) and DMON-only (11.19%) devices. These results demonstrate that the introduction of binary additives is a promising strategy to optimize active layer morphology and improve the device performance.

EXPERIMENTAL SECTION

Solar Cell Device Fabrication. The photovoltaic devices were fabricated with a structure of glass/ITO/ZnO/PBDB-T/TTC8-O1-4F/MoO_x/Ag. The ITO-coated glass substrates were cleaned using detergent, deionized water, acetone, and isopropyl alcohol under ultrasonication for 15 min each and dried by a nitrogen blow. The sol-gel ZnO were spin-coated on the substrates and annealed at 200 °C for 1 h in the air. Then, ITO substrates coated with the ZnO layer were transferred into a high purity nitrogen-filled glovebox. The mixed PBDB-T:TTC8-O1-4F was, respectively, dissolved in chlorobenzene (with 0.5 vol % DIO, 1 mg/mL DMON, and 0.5 vol % DIO and 1 mg/mL DMON) to prepare 20 mg/mL blend solutions. The mixed solutions were spin-coated onto the ITO/ZnO substrates and annealed at 140 °C for 10 min to prepare the active layers. A thin molybdenum trioxide (MoO_x) layer (10 nm) and a silver (Ag) layer (80 nm) were sequentially deposited by thermal evaporation.

ASSOCIATED CONTENT

Supporting Information

The Supporting Information is available free of charge at <https://pubs.acs.org/doi/10.1021/acsami.0c05331>.

Solar cell device characterization; general methods; synthetic route; ¹H NMR and ¹³C NMR spectra; density-functional theory calculation; CV curves; TGA and DSC diagrams; UV-vis spectra; GIWAXS patterns; electronic properties; and device optimization (PDF)

AUTHOR INFORMATION

Corresponding Author

Yongsheng Chen – State Key Laboratory and Institute of Elemento-Organic Chemistry, The Centre of Nanoscale Science and Technology and Key Laboratory of Functional Polymer Materials, Renewable Energy Conversion and Storage Center (RECAST), College of Chemistry, Nankai University, Tianjin 300071, China; orcid.org/0000-0003-1448-8177; Email: yschen99@nankai.edu.cn

Authors

Yunqian Ding – School of Materials Science and Engineering, National Institute for Advanced Materials, Nankai University, Tianjin 300350, China

Xin Zhang – State Key Laboratory and Institute of Elemento-Organic Chemistry, The Centre of Nanoscale Science and Technology and Key Laboratory of Functional Polymer Materials, Renewable Energy Conversion and Storage Center (RECAST), College of Chemistry, Nankai University, Tianjin 300071, China

Huanran Feng – State Key Laboratory and Institute of Elemento-Organic Chemistry, The Centre of Nanoscale Science and Technology and Key Laboratory of Functional Polymer Materials, Renewable Energy Conversion and Storage Center (RECAST), College of Chemistry, Nankai University, Tianjin 300071, China

Xin Ke – State Key Laboratory and Institute of Elemento-Organic Chemistry, The Centre of Nanoscale Science and Technology and Key Laboratory of Functional Polymer Materials, Renewable Energy Conversion and Storage Center (RECAST), College of Chemistry, Nankai University, Tianjin 300071, China

Lingxian Meng – State Key Laboratory and Institute of Elemento-Organic Chemistry, The Centre of Nanoscale Science and Technology and Key Laboratory of Functional Polymer Materials, Renewable Energy Conversion and Storage Center (RECAST), College of Chemistry, Nankai University, Tianjin 300071, China

Yanna Sun – State Key Laboratory and Institute of Elemento-Organic Chemistry, The Centre of Nanoscale Science and Technology and Key Laboratory of Functional Polymer Materials, Renewable Energy Conversion and Storage Center (RECAST), College of Chemistry, Nankai University, Tianjin 300071, China

Ziqi Guo – State Key Laboratory and Institute of Elemento-Organic Chemistry, The Centre of Nanoscale Science and Technology and Key Laboratory of Functional Polymer Materials, Renewable Energy Conversion and Storage Center (RECAST), College of Chemistry, Nankai University, Tianjin 300071, China

Yao Cai – State Key Laboratory and Institute of Elemento-Organic Chemistry, The Centre of Nanoscale Science and Technology and Key Laboratory of Functional Polymer Materials, Renewable Energy Conversion and Storage Center (RECAST), College of Chemistry, Nankai University, Tianjin 300071, China

Cancan Jiao – State Key Laboratory and Institute of Elemento-Organic Chemistry, The Centre of Nanoscale Science and Technology and Key Laboratory of Functional Polymer Materials, Renewable Energy Conversion and Storage Center (RECAST), College of Chemistry, Nankai University, Tianjin 300071, China

Xiangjian Wan – State Key Laboratory and Institute of Elemento-Organic Chemistry, The Centre of Nanoscale Science and Technology and Key Laboratory of Functional Polymer Materials, Renewable Energy Conversion and Storage Center (RECAST), College of Chemistry, Nankai University, Tianjin 300071, China

Chenxi Li – State Key Laboratory and Institute of Elemento-Organic Chemistry, The Centre of Nanoscale Science and Technology and Key Laboratory of Functional Polymer Materials, Renewable Energy Conversion and Storage Center (RECAST), College of Chemistry, Nankai University, Tianjin 300071, China

Nan Zheng – Institute of Polymer Optoelectronic Materials and Devices State Key Laboratory of Luminescent Materials and Devices South, China University of Technology, Guangzhou 510640, China

Zengqi Xie – Institute of Polymer Optoelectronic Materials and Devices State Key Laboratory of Luminescent Materials and Devices South, China University of Technology, Guangzhou 510640, China; orcid.org/0000-0002-9805-8176

Complete contact information is available at:
<https://pubs.acs.org/10.1021/acsami.0c05331>

Author Contributions

[†]Y.D. and X.Z. contributed equally to this work.

Funding

The authors gratefully acknowledge the financial support from MoST (2019YFA0705900 and 2016YFA0200200) and NSFC (21935007, 51873089, and 51773095) of China, Tianjin city (17JJCJC44500), and 111 Project (B12015).

Notes

The authors declare no competing financial interest.

REFERENCES

- (1) Yuan, J.; Zhang, Y.; Zhou, L.; Zhang, G.; Yip, H.-L.; Lau, T.-K.; Lu, X.; Zhu, C.; Peng, H.; Johnson, P. A.; Leclerc, M.; Cao, Y.; Ulanski, J.; Li, Y.; Zou, Y.. Single-Junction Organic Solar Cell with over 15% Efficiency Using Fused-Ring Acceptor with Electron-Deficient Core. *Joule* **2019**, *3*, 1140–1151.
- (2) Xu, X.; Feng, K.; Lee, Y. W.; Woo, H. Y.; Zhang, G.; Peng, Q. Subtle Polymer Donor and Molecular Acceptor Design Enable Efficient Polymer Solar Cells with a Very Small Energy Loss. *Adv. Funct. Mater.* **2020**, *30*, 1907570.
- (3) Zhou, Z.; Liu, W.; Zhou, G.; Zhang, M.; Qian, D.; Zhang, J.; Chen, S.; Xu, S.; Yang, C.; Gao, F.; Zhu, H.; Liu, F.; Zhu, X. Subtle molecular tailoring induces significant morphology optimization enabling over 16% efficiency organic solar cells with efficient charge generation. *Adv. Mater.* **2020**, *32*, 1906324.
- (4) Jiang, K.; Wei, Q.; Lai, J. Y. L.; Peng, Z.; Kim, H. K.; Yuan, J.; Ye, L.; Ade, H.; Zou, Y.; Yan, H. Alkyl chain tuning of small molecule acceptors for efficient organic solar cells. *Joule* **2019**, *3*, 3020–3033.
- (5) Cui, Y.; Yao, H.; Zhang, J.; Zhang, T.; Wang, Y.; Hong, L.; Xian, K.; Xu, B.; Zhang, S.; Peng, J.; Wei, Z.; Gao, F.; Hou, J. Over 16% efficiency organic photovoltaic cells enabled by a chlorinated acceptor with increased open-circuit voltages. *Nat. Commun.* **2019**, *10*, 2515.
- (6) Meng, L.; Zhang, Y.; Wan, X.; Li, C.; Zhang, X.; Wang, Y.; Ke, X.; Xiao, Z.; Ding, L.; Xia, R.; Yip, H.-L.; Cao, Y.; Chen, Y. Organic and solution-processed tandem solar cells with 17.3% efficiency. *Science* **2018**, *361*, 1094–1098.
- (7) Zhan, L.; Li, S.; Lau, T.-K.; Cui, Y.; Lu, X.; Shi, M.; Li, C.-Z.; Li, H.; Hou, J.; Chen, H. Over 17% efficiency ternary organic solar cells enabled by two non-fullerene acceptors working in alloy-like model. *Energy Environ. Sci.* **2020**, *13*, 635–645.
- (8) Liu, L.; Kan, Y.; Gao, K.; Wang, J.; Zhao, M.; Chen, H.; Zhao, C.; Jiu, T.; Jen, A.-K.-Y.; Li, Y. Graphdiyne Derivative as Multifunctional Solid Additive in Binary Organic Solar Cells with 17.3% Efficiency and High Reproducibility. *Adv. Mater.* **2020**, *32*, 1907604.
- (9) Lin, Y.; Adilbekova, B.; Firdaus, Y.; Yengel, E.; Faber, H.; Sajjad, M.; Zheng, X.; Yarali, E.; Seitkhan, A.; Bakr, O. M.; El-Labban, A.; Schwingenschlogl, U.; Tung, V.; McCulloch, I.; Laquai, F.; Anthopoulos, T. D. 17% Efficient Organic Solar Cells Based on Liquid Exfoliated WS₂ as a Replacement for PEDOT:PSS. *Adv. Mater.* **2019**, *31*, 1902965.
- (10) Liu, Q.; Jiang, Y.; Jin, K.; Qin, J.; Xu, J.; Li, W.; Xiong, J.; Liu, J.; Xiao, Z.; Sun, K.; Yang, S.; Zhang, X.; Ding, L. 18% Efficiency organic solar cells. *Sci. Bull.* **2020**, *65*, 272–275.
- (11) Huang, F. Organic Tandem Cells with PCE over 17%. *Acta Polym. Sin.* **2018**, *9*, 1141–1143.
- (12) Qiu, N.; Zhang, H.; Wan, X.; Li, C.; Ke, X.; Feng, H.; Kan, B.; Zhang, H.; Zhang, Q.; Lu, Y.; Chen, Y. A New Nonfullerene Electron Acceptor with a Ladder Type Backbone for High-Performance Organic Solar Cells. *Adv. Mater.* **2017**, *29*, 1604964.
- (13) Zhang, Y.; Kan, B.; Sun, Y.; Wang, Y.; Xia, R.; Ke, X.; Yi, Y. Q. Q.; Li, C.; Yip, H. L.; Wan, X.; Cao, Y.; Chen, Y. Nonfullerene tandem organic solar cells with high performance of 14.11%. *Adv. Mater.* **2018**, *30*, 1707508.
- (14) Kan, B.; Zhang, J.; Liu, F.; Wan, X.; Li, C.; Ke, X.; Wang, Y.; Feng, H.; Zhang, Y.; Long, G.; Friend, R. H.; Bakulin, A. A.; Chen, Y. Fine-tuning the energy levels of a nonfullerene small-molecule acceptor to achieve a high short-circuit current and a power conversion efficiency over 12% in organic solar cells. *Adv. Mater.* **2018**, *30*, 1704904.

- (15) Lin, H.; Chen, S.; Li, Z.; Lai, J. Y. L.; Yang, G.; McAfee, T.; Jiang, K.; Li, Y.; Liu, Y.; Hu, H.; Zhao, J.; Ma, W.; Ade, H.; Yan, H. High-Performance Non-Fullerene Polymer Solar Cells Based on a Pair of Donor-Acceptor Materials with Complementary Absorption Properties. *Adv. Mater.* **2015**, *27*, 7299–7304.
- (16) Cai, Y.; Meng, L.; Gao, H.; Guo, Z.; Zheng, N.; Xie, Z.; Zhang, H.; Wan, X.; Chen, Y. Achieving Organic Solar Cells with Efficiency over 14% Based on a Non-Fullerene Acceptor incorporating the Cyclopentathiophene Unit Fused Backbone. *J. Mater. Chem. A* **2020**, *8*, 5194–5199.
- (17) Zhang, X.; Ding, Y.; Wan, X.; Ke, X.; Li, C.; Chen, Y. A Novel Acceptor with a N, N-dialkyl thieno [3', 2': 2, 3] indolo [7, 6-g] thieno [3, 2-b] indole (TITI) Core for Organic Solar Cells with a high Fill Factor of 0.75. *Chem. Commun.* **2020**, *56*, 751–753.
- (18) Hong, L.; Yao, H.; Yu, R.; Xu, Y.; Gao, B.; Ge, Z.; Hou, J. Investigating the Trade-Off between Device Performance and Energy Loss in Nonfullerene Organic Solar Cells. *ACS Appl. Mater. Interfaces* **2019**, *11*, 29124–29131.
- (19) Luo, Z.; Zhao, Y.; Zhang, Z.-G.; Li, G.; Wu, K.; Xie, D.; Gao, W.; Li, Y.; Yang, C. Side-Chain Effects on Energy-Level Modulation and Device Performance of Organic Semiconductor Acceptors in Organic Solar Cells. *ACS Appl. Mater. Interfaces* **2017**, *9*, 34146–34152.
- (20) Feng, L.; Yuan, J.; Zhang, Z.; Peng, H.; Zhang, Z.-G.; Xu, S.; Liu, Y.; Li, Y.; Zou, Y. Thieno[3,2-b]pyrrolo-Fused Pentacyclic Benzotriazole-Based Acceptor for Efficient Organic Photovoltaics. *ACS Appl. Mater. Interfaces* **2017**, *9*, 31985–31992.
- (21) Zhang, Y.; Wang, Y.; Yang, T.; Liu, T.; Xiao, Y.; Lu, X.; Yan, H.; Yuan, Z.; Chen, Y.; Li, Y. Thioether Bond Modification Enables Boosted Photovoltaic Performance of Nonfullerene Polymer Solar Cells. *ACS Appl. Mater. Interfaces* **2019**, *11*, 32218–32224.
- (22) Li, G.; Xu, C.; Luo, Z.; Ning, W.; Liu, X.; Gong, S.; Zou, Y.; Zhang, F.; Yang, C. Novel Nitrogen-Containing Heterocyclic Non-Fullerene Acceptors for Organic Photovoltaic Cells: Different End-Capping Groups Leading to a Big Difference of Power Conversion Efficiencies. *ACS Appl. Mater. Interfaces* **2020**, *12*, 13068–13076.
- (23) Wang, Y.; Zhang, Y.; Qiu, N.; Feng, H.; Gao, H.; Kan, B.; Ma, Y.; Li, C.; Wan, X.; Chen, Y. A halogenation strategy for over 12% efficiency nonfullerene organic solar cells. *Adv. Energy Mater.* **2018**, *8*, 1702870.
- (24) Feng, H.; Yi, Y. Q.; Ke, X.; Yan, J.; Zhang, Y.; Wan, X.; Li, C.; Zheng, N.; Xie, Z.; Chen, Y. New Anthracene-Fused Nonfullerene Acceptors for High-Efficiency Organic Solar Cells: Energy Level Modulations Enabling Match of Donor and Acceptor. *Adv. Energy Mater.* **2019**, *9*, 1803541.
- (25) Feng, H.; Qiu, N.; Wang, X.; Wang, Y.; Kan, B.; Wan, X.; Zhang, M.; Xia, A.; Li, C.; Liu, F.; Zhang, H.; Chen, Y. An A-D-A type small-molecule electron acceptor with end-extended conjugation for high performance organic solar cells. *Chem. Mater.* **2017**, *29*, 7908–7917.
- (26) Kan, B.; Feng, H.; Wan, X.; Liu, F.; Ke, X.; Wang, Y.; Wang, Y.; Zhang, H.; Li, C.; Hou, J.; Chen, Y. Small molecule acceptor based on the heptacyclic benzodi(cyclopentadithiophene) unit for high efficient non-fullerene organic solar cells. *J. Am. Chem. Soc.* **2017**, *139*, 4929–4934.
- (27) Li, M.; Liu, Y.; Ni, W.; Liu, F.; Feng, H.; Zhang, Y.; Liu, T.; Zhang, H.; Wan, X.; Kan, B.; Zhang, Q.; Russell, T. P.; Chen, Y. A simple small molecule as an acceptor for fullerene-free organic solar cells with efficiency near 8%. *J. Mater. Chem. A* **2016**, *4*, 10409–10413.
- (28) Hoven, C. V.; Dang, X.-D.; Coffin, R. C.; Peet, J.; Nguyen, T.-Q.; Bazan, G. C. Improved performance of polymer bulk heterojunction solar cells through the reduction of phase separation via solvent additives. *Adv. Mater.* **2010**, *22*, No. E63.
- (29) Peet, J.; Kim, J. Y.; Coates, N. E.; Ma, W. L.; Moses, D.; Heeger, A. J.; Bazan, G. C. Efficiency Enhancement in Low-Bandgap Polymer Solar Cells by Processing with Alkane Dithiols. *Nat. Mater.* **2007**, *6*, 497–500.
- (30) Li, G.; Shrotriya, V.; Huang, J.; Yao, Y.; Moriarty, T.; Emery, K.; Yang, Y. High-Efficiency Solution Processable Polymer Photovoltaic Cells by Self-Organization of Polymer Blends. *Nat. Mater.* **2005**, *4*, 864–868.
- (31) McDowell, C.; Abdelsamie, M.; Toney, M. F.; Bazan, G. C. Solvent additives: key morphology-directing agents for solution-processed organic solar cells. *Adv. Mater.* **2018**, *30*, 1707114.
- (32) Lee, J. K.; Ma, W. L.; Yuen, J.; Moon, J. S.; Kim, J. Y.; Lee, K.; Bazan, G. C.; Heeger, A. J. Processing additives for improved efficiency from bulk heterojunction solar cells. *J. Am. Chem. Soc.* **2008**, *130*, 3619–3623.
- (33) Huang, Y.; Kramer, E. J.; Heeger, A. J.; Bazan, G. C. Bulk heterojunction solar cells: morphology and performance relationships. *Chem. Rev.* **2014**, *114*, 7006–7043.
- (34) An, Y.; Liao, X.; Chen, L.; Yin, J.; Ai, Q.; Xie, Q.; Huang, B.; Liu, F.; Jen, A. K. Y.; Chen, Y. Nonhalogen Solvent-Processed Asymmetric Wide-Bandgap Polymers for Nonfullerene Organic Solar Cells with Over 10% Efficiency. *Adv. Funct. Mater.* **2018**, *28*, 1706517.
- (35) Xiong, Y.; Ye, L.; Gadisa, A.; Zhang, Q.; Rech, J. J.; You, W.; Ade, H. Revealing the Impact of F4-TCNQ as Additive on Morphology and Performance of High-Efficiency Nonfullerene Organic Solar Cells. *Adv. Funct. Mater.* **2019**, *29*, 1806262.
- (36) Lim, B.; Jo, J.; Na, S.-L.; Kim, J.; Kim, S.-S.; Kim, D.-Y. A morphology controller for high-efficiency bulk-heterojunction polymer solar cells. *J. Mater. Chem.* **2010**, *20*, 10919–10923.
- (37) Liu, Y.; Wan, X.; Yin, B.; Zhou, J.; Long, G.; Yin, S.; Chen, Y. Efficient solution processed bulk-heterojunction solar cells based a donor-acceptor oligothiophene. *J. Mater. Chem.* **2010**, *20*, 2464–2468.
- (38) Zhao, F.; Wang, C.; Zhan, X. Morphology control in organic solar cells. *Adv. Energy Mater.* **2018**, *8*, 1703147.
- (39) Dong, S.; Zhang, K.; Xie, B.; Xiao, J.; Yip, H.-L.; Yan, H.; Huang, F.; Cao, Y. High-Performance Large-Area Organic Solar Cells Enabled by Sequential Bilayer Processing via Nonhalogenated Solvents. *Adv. Energy Mater.* **2019**, *9*, 1802832.
- (40) Zhao, J.; Li, Y.; Yang, G.; Jiang, K.; Lin, H.; Ade, H.; Ma, W.; Yan, H. Efficient organic solar cells processed from hydrocarbon solvents. *Nat. Energy* **2016**, *1*, 15027.
- (41) Lin, Y.; Zhao, F.; He, Q.; Huo, L.; Wu, Y.; Parker, T. C.; Ma, W.; Sun, Y.; Wang, C.; Zhu, D.; Heeger, A. J.; Marder, S. R.; Zhan, X. High-performance electron acceptor with thienyl side chains for organic photovoltaics. *J. Am. Chem. Soc.* **2016**, *138*, 4955–4961.
- (42) Guo, B.; Guo, X.; Li, W.; Meng, X.; Ma, W.; Zhang, M.; Li, Y. A Wide-Bandgap Conjugated Polymer for highly Efficient Inverted Single and Tandem Polymer Solar Cells. *J. Mater. Chem. A* **2016**, *4*, 13251–13258.
- (43) Liu, F.; Zhou, Z.; Zhang, C.; Vergote, T.; Fan, H.; Liu, F.; Zhu, X. A thieno[3,4-b]thiophene-based non-fullerene electron acceptor for high-performance bulk-heterojunction organic solar cells. *J. Am. Chem. Soc.* **2016**, *138*, 15523–15526.
- (44) Wan, Q.; Guo, X.; Wang, Z.; Li, W.; Guo, B.; Ma, W.; Zhang, M.; Li, Y. 10.8% Efficiency polymer solar cells based on ptb7-th and PC71BM via binary solvent additives treatment. *Adv. Funct. Mater.* **2016**, *26*, 6635–6640.
- (45) Graham, K. R.; Wieruszewski, P. M.; Stalder, R.; Hartel, M. J.; Mei, J.; So, F.; Reynolds, J. R. Improved Performance of Molecular Bulk-Heterojunction Photovoltaic Cells through Predictable Selection of Solvent Additives. *Adv. Funct. Mater.* **2012**, *22*, 4801–4813.
- (46) Schmidt, K.; Tassone, C. J.; Niskala, J. R.; Yiu, A. T.; Lee, O. P.; Weiss, T. M.; Wang, C.; Fréchet, J. M. J.; Beaujuge, P. M.; Toney, M. F. A mechanistic understanding of processing additive induced efficiency enhancement in bulk heterojunction organic solar cells. *Adv. Mater.* **2014**, *26*, 300–305.
- (47) Yu, R.; Yao, H.; Hong, L.; Qin, Y.; Zhu, J.; Cui, Y.; Li, S.; Hou, J. Design and application of volatilizable solid additives in non-fullerene organic solar cells. *Nat. Commun.* **2018**, *9*, 4645.
- (48) Yu, R.; Yao, H.; Chen, Z.; Xin, J.; Hong, L.; Xu, Y.; Zu, Y.; Ma, W.; Hou, J. Enhanced pi-pi Interactions of Nonfullerene Acceptors by

Volatilizable Solid Additives in Efficient Polymer Solar Cells. *Adv. Mater.* **2019**, *31*, 1900477.

(49) Chen, J.; Bi, Z.; Xu, X.; Zhang, Q.; Yang, S.; Guo, S.; Yan, H.; You, W.; Ma, W. Fine optimization of morphology evolution kinetics with binary additives for efficient non-fullerene organic solar cells. *Adv. Sci.* **2019**, *6*, 1801560.

(50) Jung, Y.-S.; Yeo, J.-S.; Kim, N.-K.; Lee, S.; Kim, D.-Y. Selective morphology control of bulk heterojunction in polymer solar cells using binary processing additives. *ACS Appl. Mater. Interfaces* **2016**, *8*, 30372–30378.

(51) Wang, D. H.; Kyaw, A. K. K.; Pouliot, J.-R.; Leclerc, M.; Heeger, A. J. Enhanced power conversion efficiency of low bandgap polymer solar cells by insertion of optimized binary processing additives. *Adv. Energy Mater.* **2014**, *4*, 1300835.

(52) He, D.; Zhao, F.; Xin, J.; Rech, J. J.; Wei, Z.; Ma, W.; You, W.; Li, B.; Jiang, L.; Li, Y.; Wang, C. A fused ring electron acceptor with decacyclic core enables over 13.5% efficiency for organic solar cells. *Adv. Energy Mater.* **2018**, *8*, 1802050.

(53) Opoku, H.; Lim, B.; Shin, E. S.; Kong, H.; Park, J. M.; Bathula, C.; Noh, Y. Y. Bis-Diketopyrrolopyrrole and Carbazole-Based Terpolymer for High Performance Organic Field-Effect Transistors and Infra-Red Photodiodes. *Macromol. Chem. Phys.* **2019**, *220*, 1900287.

(54) Yao, Y.; Hou, J.; Xu, Z.; Li, G.; Yang, Y. Effects of Solvent Mixtures on the Nanoscale Phase Separation in Polymer Solar Cells. *Adv. Funct. Mater.* **2008**, *18*, 1783–1789.

(55) Gao, H.-H.; Sun, Y.; Cai, Y.; Wan, X.; Meng, L.; Ke, X.; Li, S.; Zhang, Y.; Xia, R.; Zheng, N.; Xie, Z.; Li, C.; Zhang, M.; Yip, H. L.; Cao, Y.; Chen, Y. Achieving Both Enhanced Voltage and Current through Fine-Tuning Molecular Backbone and Morphology Control in Organic Solar Cells. *Adv. Energy Mater.* **2019**, *9*, 1901024.

(56) Sun, Y.; Gao, H.-H.; Yi, Y.-Q.; Wan, X.; Feng, H.; Ke, X.; Zhang, Y.; Yan, J.; Li, C.; Chen, Y. Fluorination-Modulated End Units for High-Performance Non-Fullerene Acceptors Based Organic Solar Cells. *Sci. China Mater.* **2019**, *62*, 1210–1217.

(57) Zhao, W.; Qian, D.; Zhang, S.; Li, S.; Inganas, O.; Gao, F.; Hou, J. Fullerene-free polymer solar cells with over 11% efficiency and excellent thermal stability. *Adv. Mater.* **2016**, *28*, 4734.

(58) Park, S. H.; Roy, A.; Beaupre, S.; Cho, S.; Coates, N.; Moon, J. S.; Moses, D.; Leclerc, M.; Lee, K.; Heeger, A. J. Bulk Heterojunction Solar Cells with Internal Quantum Efficiency Approaching 100%. *Nat. Photonics* **2009**, *3*, 297–302.

(59) Hexemer, A.; Bras, W.; Glossinger, J.; Schaible, E.; Gann, E.; Kirian, R.; MacDowell, A.; Church, M.; Rude, B.; Padmore, H. A SAXS/WAXS/GISAXS Beamline with Multilayer Monochromator. *J. Phys.: Conf. Ser.* **2010**, *247*, 012007.

(60) Blom, P. W. M.; Mihailetchi, V. D.; Koster, L. J. A.; Markov, D. E. Device Physics of Polymer: Fullerene Bulk Heterojunction Solar Cells. *Adv. Mater.* **2007**, *19*, 1551–1566.

(61) Brabec, C. J.; Gowrisanker, S.; Halls, J. J. M.; Laird, D.; Jia, S.; Williams, S. P. Polymer–Fullerene Bulk-Heterojunction Solar Cells. *Adv. Mater.* **2010**, *22*, 3839–3856.

(62) Riedel, I.; Parisi, J.; Dyakonov, V.; Lutsen, L.; Vanderzande, D.; Hummelen, J. C. Effect of Temperature and Illumination on the Electrical Characteristics of Polymer–Fullerene Bulk-Heterojunction Solar Cells. *Adv. Funct. Mater.* **2004**, *14*, 38–44.

(63) Proctor, C. M.; Love, J. A.; Nguyen, T.-Q. Mobility Guidelines for High Fill Factor Solution-Processed Small Molecule Solar Cells. *Adv. Mater.* **2014**, *26*, 5957–5961.

(64) Zhao, W.; Li, S.; Yao, H.; Zhang, S.; Zhang, Y.; Yang, B.; Hou, J. Molecular Optimization Enables over 13% Efficiency in Organic Solar Cells. *J. Am. Chem. Soc.* **2017**, *139*, 7148–7151.